



Article

Electrochemistry of Rhodanine Derivatives as Model for New Colorimetric and Electrochemical Azulene Sensors for the Detection of Heavy Metal Ions

Ovidiu-Teodor Matica ¹, Cornelia Musina (Borsaru) ¹, Alina Giorgiana Brotea ¹, Eleonora-Mihaela Ungureanu ^{1,*}, Mihaela Cristea ², Raluca Isopescu ³, George-Octavian Buica ³ and Alexandru C. Razus ²

¹ Doctoral School of Chemical Engineering and Biotechnologies, University “Politehnica” of Bucharest, Gheorghe Polizu 1–7, Sector 1, 011061 Bucharest, Romania; maticaovidiu@yahoo.co.uk (O.-T.M.)

² “C. D. Nenitzescu” Institute of Organic and Supramolecular Chemistry of the Romanian Academy, 71141 Bucharest, Romania

³ Faculty of Chemical Engineering and Biotechnologies, University “Politehnica” of Bucharest, Gheorghe Polizu 1–7, Sector 1, 011061 Bucharest, Romania

* Correspondence: em_ungureanu2000@yahoo.com

Abstract: Rhodanine (**R**) is a heterocycle having complexing properties for heavy metal (HM) ions. Considering the similar electron-donating character of diethylaminobenzene and azulene, electrochemical characterization of (Z)-5-(azulen-1-ylmethylene)-2-thioxo-thiazolidin-4-one (**R1**) and 5-(4-diethylamino-benzylidene)-2-thioxo-thiazolidin-4-one (**R2**) was performed to establish their common features. Chemically modified electrodes based on **R1** and **R2** were compared for HM recognition. Evidence for the formation of films was provided by scanning and controlled potential electrolysis, and HM recognition experiments were performed using their films. Parallel studies for analysis of HMs by complexation in solution were performed by UV-Vis. The analogy between **R1** and **R2** created the premise for easier selection of compounds for certain applications. The performance of the chemically modified electrodes was evaluated as detection limits for HMs. The azulene monomer (**R1**) proved to be the best candidate for Pb(II) detection, being about eight times more sensitive than **R2**. However, in solution, **R2** proved to be a good choice for optical measurements, having a higher absorption coefficient. These results support the two ligands having different behaviors in homogeneous and heterogeneous systems.

Keywords: advanced materials; rhodanine; azulene; diethylaminobenzene; colorimetric and electrochemical sensors; heavy metal



Citation: Matica, O.-T.; Musina (Borsaru), C.; Brotea, A.G.; Ungureanu, E.-M.; Cristea, M.; Isopescu, R.; Buica, G.-O.; Razus, A.C. Electrochemistry of Rhodanine Derivatives as Model for New Colorimetric and Electrochemical Azulene Sensors for the Detection of Heavy Metal Ions. *Symmetry* **2023**, *15*, 752. <https://doi.org/10.3390/sym15030752>

Academic Editor:
Christophe Humbert

Received: 1 March 2023
Revised: 14 March 2023
Accepted: 16 March 2023
Published: 18 March 2023



Copyright: © 2023 by the authors. Licensee MDPI, Basel, Switzerland. This article is an open access article distributed under the terms and conditions of the Creative Commons Attribution (CC BY) license (<https://creativecommons.org/licenses/by/4.0/>).

1. Introduction

2-Sulfanilidene-1,3-thiazolidin-4-one (rhodanine, **R**) is a 5-membered ring heterocyclic organic ring with sulfur and nitrogen in the positions 1 and 3 (Figure 1). Some rhodanine-substituted derivatives are used as highly sensitive reagents for the determination of metal ions in analytical chemistry [1–3]. These derivatives are encountered in drug production and applied in the treatment of cancer and diabetes [4,5], as antimicrobial compounds [4–6], or as pan-assay interference compounds (PAINS), which give false positive results for biological samples [6–8]. Another category of applications of these compounds is their use in preparing polymer layers to protect various surfaces against corrosion [9]. Their efficiency as organic corrosion inhibitors is due to heteroatoms with high electron density, such as nitrogen, sulphur, or multiple bonds, acting as adsorption centres [10]. Rhodanines generate protective polymeric films against corrosion by physical and chemical adsorption, thereby reducing corrosive attack on mild steel [11,12] or copper [9,13,14]. Last but not least, due to their conductive properties, these films are used in the achievement of photovoltaic cells [15], with refs. [15–17] demonstrating improved solar energy capture efficiency.

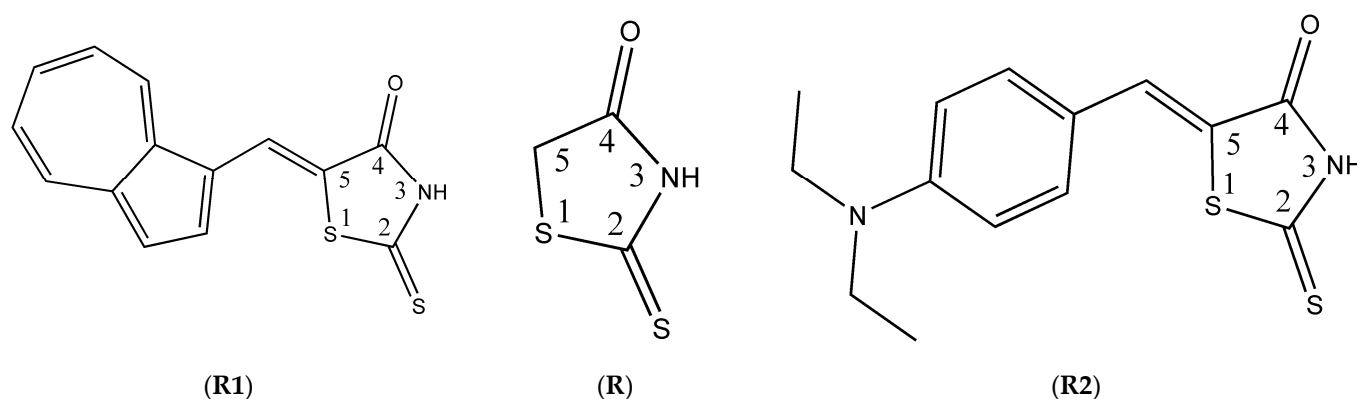


Figure 1. Structures of (Z)-5-(azulen-1-ylmethylene)-2-thioxo-thiazolidin-4-one (**R1**), 2-thioxo-thiazolidin-4-one (**R**), and 5-(4 diethylamino-benzylidene)-2-thioxo-thiazolidin-4-one (**R2**).

The polymerization of **R** and its derivatives has been reported [9–14] and several practical applications are mentioned. Polyrhodanine films were obtained by electrochemical oxidation of rhodanine solutions in water [18,19] or organic media [20]. The polyrhodanine films synthesized so far have been shown to have good properties, such as high thermal stability and adequate solubility in common organic solvents, indicating their potential use as protective films for metallic or insulating surfaces and other materials [18].

This work is focused on the comparison of (Z)-5-(azulen-1-ylmethylene)-2-thioxo-thiazolidin-4-one (**R1**) and diethylaminobenzylidenerhodanine (**R2**). Compound **R1** contains an azulene-1-yl moiety (Figure 1). Azulene is a non-alternating bicyclic aromatic hydrocarbon with an electron-deficient seven-carbon ring (tropylium cation ion configuration) fused to an electron-rich five-carbon ring (cyclopentadienyl anion configuration), which assigns a relatively large dipole moment (1.08 D) to this molecule. The electrochemical, optical, and photophysical properties of differently substituted azulene derivatives can vary significantly depending on the position and nature of the substituent [21–24]. The structure of compound **R2** contains a phenyl substituted in the *para* position with a diethylamino group and has a polarity similar [25] to that of azulene (dipole moment 1.61 D for dimethylaminobenzene).

Azulene derivatives of **R**, such as **R1**, proved to be systems with high affinity for cations, with the push–pull structure being favourable for the construction of modified electrodes with complexing properties. Previous research on **R1** [26] highlighted the electrochemical processes of this compound at anodic and cathodic potentials and the easy formation of films with complexing properties. Starting from **R1**, chemically modified electrodes (CMEs) were prepared [26]. They were tested for the analysis of HMs with good results [26]. This confirmed the literature data showing that azulene derivatives of **R**, known for their complexing properties towards HMs [26], can be used in the determination of metals, similar to the use of *p*-dimethylaminophenylene rhodanine for the accurate analysis of Ni, Cu, Zn, and Fe ions [27] or triarylamine rhodanine derivatives used for the detection of Ag(I) and Hg(II) ions by colorimetric methods [28,29].

Azulenenic compounds require special conditions during synthesis to protect the azulenic moiety, which is easily oxidizable. The analogy between the azulene derivative of rhodanine and the aromatic *p*-dialkylaminobenzylidene rhodanine may provide a basis for preliminary testing of these more accessible compounds. Thus, the selection of compounds of interest with interesting properties for a specific application will be facilitated. This approach can reduce the costs associated with the discovery of new compounds (expensive reagents, working time under special conditions), which is generally the case for azulene derivatives.

Comparison of the electrochemical study of these compounds (Figure 1) revealed the similarity between the electrochemical processes of oxidation and reduction, which confirmed the similarity of the chemical properties of the two compounds [24] and was

obvious considering the similar electron-donating character of the structures of **R1** and **R2**. Consequently, their affinities for cations were expected to be similar. To evidence the similarity between the two ligands, some previous results referring to **R1** [30] were used and a thorough study of **R2** was carried out. The possibility of comparing these push–pull structures to build modified electrodes with complexation properties for HMs was also investigated for **R2** and compared with that of **R1**. Parallel studies of HM complexation in solution by **R1** and **R2** were performed by UV-Vis.

2. Materials and Methods

(Z)-5-(Azulen-1-yl)methylene)-2-thioxothiazolidin-4-one (**R1**) was synthesized according to the literature [31]. Diethylaminobenzylidenerhodanine (**R2**) was purchased from LOBA CHEMIE (98%). All other reagents for voltammetric experiments were analytical grade. Acetonitrile, used as the solvent, was electronic grade 99.999% (Sigma Aldrich, St. Louis, MI, USA) and tetra-*n*-butylammonium perchlorate (Flukapuriss) was electrochemical grade 99%. These reagents were used as the solvent and supporting electrolyte, without further purification. Mercury(II) acetate (Fluka, Munich, Germany, $\geq 98\%$), copper(II) acetate monohydrate (Fluka, Munich, Germany, $\geq 98\%$), lead(II) nitrate (Fluka, Munich, Germany, $\geq 99.5\%$), and cadmium nitrate tetrahydrate (Fluka, Munich, Germany, $\geq 98\%$) were used for the recognition experiments.

The electrochemical experiments for ligand characterization and preparation of modified electrodes were performed by cyclic voltammetry (CV), differential pulse voltammetry (DPV), and rotating disk electrode voltammetry (RDE). The experiments were performed in a three-compartment cell coupled to a PGSTAT 12 AUTOLAB potentiostat. The working electrode (WE) was a glassy carbon (GC) disc with a diameter of 3 mm. GS was thoroughly prepared for each determination by polishing its surface with diamond paste (0.25 μm) and then rinsed with acetonitrile with acetonitrile. The reference electrode (RE) was Ag/10 mmol·L⁻¹ AgNO₃ in 0.1 mol·L⁻¹ tetra-*n*-butylammonium perchlorate (TBAP) in acetonitrile (CH₃CN) and a platinum wire was used as the auxiliary electrode (AE). For the HM recognition experiments, a transfer cell with a Pt wire was used as the AE and Ag/Ag Cl, KCl 3 M was used as the RE.

CV curves were generally recorded at a scan rate of 0.1 V·s⁻¹. The DPV curves were recorded at 0.01 V·s⁻¹ with a pulse height of 0.025 V and a step time of 0.2 s. The RDE curves were recorded at 0.01 V·s⁻¹. After the experiment, the potentials were related to the potential of the ferrocene/ferrocenium redox couple (Fc/Fc⁺) for the purpose of comparisons. All electrochemical characterization experiments were performed under an argon atmosphere. The experiments were performed at room temperature (25 °C).

The chemically modified electrodes (CMEs) were prepared from millimolar ligand solutions in 0.1 M TBAP/CH₃CN by scanning or controlled potential electrolysis (CPE). Then, each modified electrode was washed with acetonitrile and placed in 0.1 M acetate buffer solution (pH = 4.5) where it was equilibrated and overoxidized following a procedure similar to that previously described [30,31]. The CMEs were tested as HM sensors in aqueous medium using the transfer cell that had the CME as the WE. Each CME was immersed for 10 (15) minutes under stirring in synthetic HM ion solutions. For recognition experiments using chemically modified electrodes or UV-Vis, the metal ion solutions were prepared from 10⁻³ M stock solutions of mercury(II) acetate, copper(II) acetate monohydrate, lead(II) nitrate, and cadmium nitrate tetrahydrate. Afterwards, the electrode was removed and rinsed with deionized water, then immersed in a cell containing 0.1 M acetate buffer solution (pH = 4.5). Here, it was kept for 3 min at -1.0 V, and then the DPV curve was recorded between -1.0 and +0.6 V.

The UV-Vis spectrometry study was performed on a JASCO V-670 in 1 cm optical path quartz cuvettes in freshly dried acetonitrile. Aliquots of heavy metal solutions were added to the ligand solution and UV-Vis spectra were recorded between 800 and 200 nm one minute after each addition.

3. Results

3.1. Electrochemical Characterization of the Ligands

The electrochemical behavior of the used ligands was studied in millimolar solutions in supporting electrolyte (0.1 M TBAP, CH₃CN) by electrochemical methods. Ligand solutions were obtained by successively diluting the initial solution, of higher concentration, with the appropriate amount of supporting electrolyte solution. The curves for reduction and oxidation processes were recorded starting from the equilibrium potential. For each electrochemical method used to characterize the ligands, voltammograms were recorded for the supporting electrolyte (with zero ligand concentration); their curves were shown with dashed lines. The peaks of the cathodic and anodic processes were denoted in the order in which they appeared in the DPV voltammograms. To be able to compare the values of the cathodic and anodic currents more easily, the currents for the cathodic processes were represented in absolute values.

3.1.1. Characterization of the Ligands by Cyclic Voltammetry

Characterization by cyclic voltammetry (CV) was performed in solutions of different concentrations (Figure 2), at different scan rates (Figure 3), and on different potential domains (Figure 4). For **R1** ligand, 5 peaks corresponding to 5 reduction processes on the cathodic domain and 2 peaks corresponding to 2 oxidation processes on the anodic domain were identified [30]. For ligand **R2**, 3 peaks corresponding to 3 reduction processes on the cathodic domain and 5 peaks corresponding to 5 oxidation processes on the anodic domain were identified. Figure S1 shows the maximum values of the peak currents as a function of the ligand concentration in the solution, and in Table S1 the equations of the correlation lines are given. Figure 3b shows the variation of the peak currents for processes a1 and c1, respectively, with the square root of the scan rate. The equations of the correlation lines between the two quantities are given in Table 1. The peak potentials are given in Table 2.

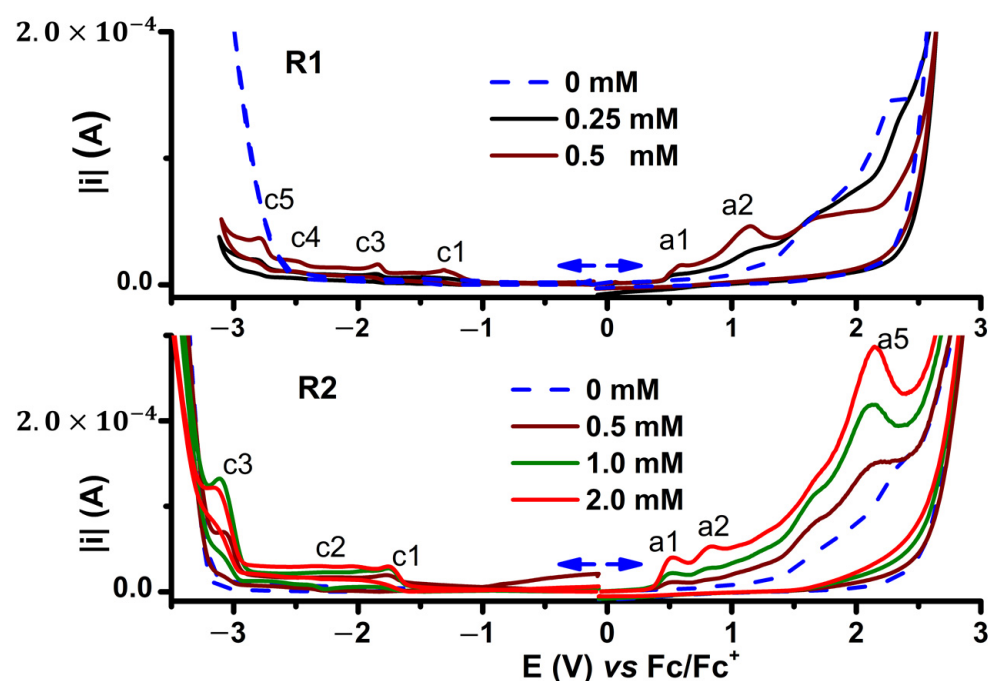


Figure 2. CV (0.1 Vs^{-1}) anodic and cathodic curves (with currents in absolute values) on GC for **R1** and **R2** in 0.1 M TBAP/CH₃CN at different concentrations; a1–a5 and c1–c5 are the anodic and cathodic peaks, respectively.

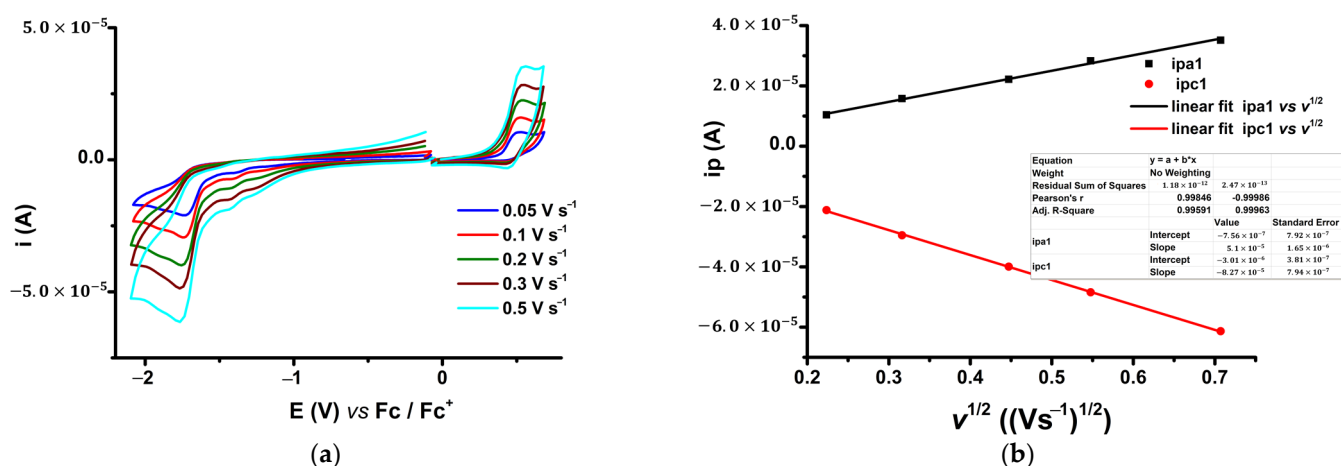


Figure 3. CV curves for 1 mM solution of **R2** in 0.1 M TBAP/CH₃CN at different scan rates (a); a1 and c1 current peak variations with the square root of the scan rate (b).

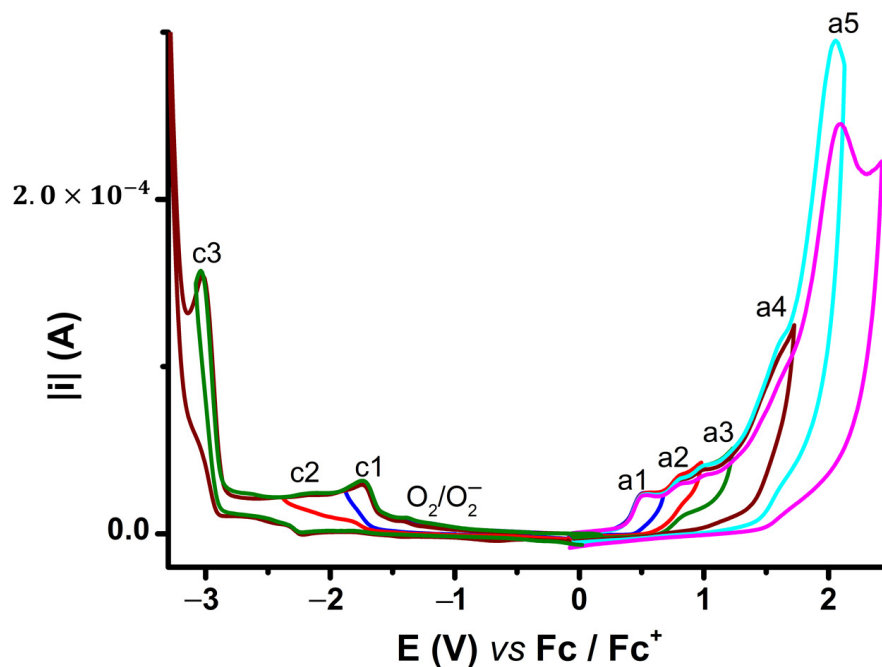


Figure 4. CV curves (0.1 V s^{-1}) on GC at different potential domains for 1 mM solutions in 0.1 M TBAP/CH₃CN for **R2**; a1–a5 and c1–c3 are the anodic and cathodic peaks, respectively.

Table 1. Linear dependence of first anodic (a1) and cathodic (c1) peak currents (in A) on the square root of the scan rate (in $\text{V} \cdot \text{s}^{-1}$).

Ligand	Process	Equation	Adj. R-Square	Reference
R1	a1	$ipa1 = -3.80 \times 10^{-6} + 44.67 \times 10^{-6} \times \sqrt{v}$	0.998	[32]
R2	a1	$ipa1 = -7.56 \times 10^{-7} + 51.6 \times 10^{-6} \times \sqrt{v}$	0.996	this paper
	c1	$ipc1 = -3.01 \times 10^{-7} - 82.7 \times 10^{-6} \times \sqrt{v}$	0.999	this paper

Table 2. Anodic and cathodic process assignments for **R2** peak potentials (V vs. Fc/Fc⁺) from CV and DPV curves and half-wave potential ($E_{1/2}$) values from RDE.

Process	Method			Process Assignment
	CV	DPV	RDE ($E_{1/2}$)	
a1	0.526 <i>qr</i>	0.436	<i>sh</i>	Radical cation formation from amino group
a2	0.840 <i>i</i>	0.753	"peak" at 0.90	Oligomer oxidation
a3	<i>i</i>	1.191	-	
a4	<i>qr</i>	1.518	-	
a5	2.147 <i>i</i>	1.800	-	
c1	-1.759 <i>qr</i>	-1.711	-1.70	Reduction of C=C double bond
c2	<i>i</i>	-2.217	-2.20	-
c3	-3.151 <i>qr</i>	-3.011	-3.10 **	Reduction of C=S bond

qr—quasi-reversible process, *i*—irreversible process; *sh*—shoulder; ** revealed only for low **R2** concentration (0.5 mM).

3.1.2. Characterization of Ligands by Differential Pulse Voltammetry

Characterization by DPV was performed in solutions of different concentrations (Figure 5). Five peaks on the cathodic domain and 2 peaks on the anodic domain corresponding to the oxidation/reduction processes of **R1** ligand were noticed [30]. For **R2** ligand, 3 peaks on the cathodic domain and 5 peaks on the anodic domain were identified. Figure S2 shows the maximum values of the DPV peak currents depending on the ligand concentration in solution, and Table S2 shows the equations of the correlation lines. To correlate the processes highlighted in CV and DPV, the voltammograms for ligand **R2** were represented in parallel in Figure S3.

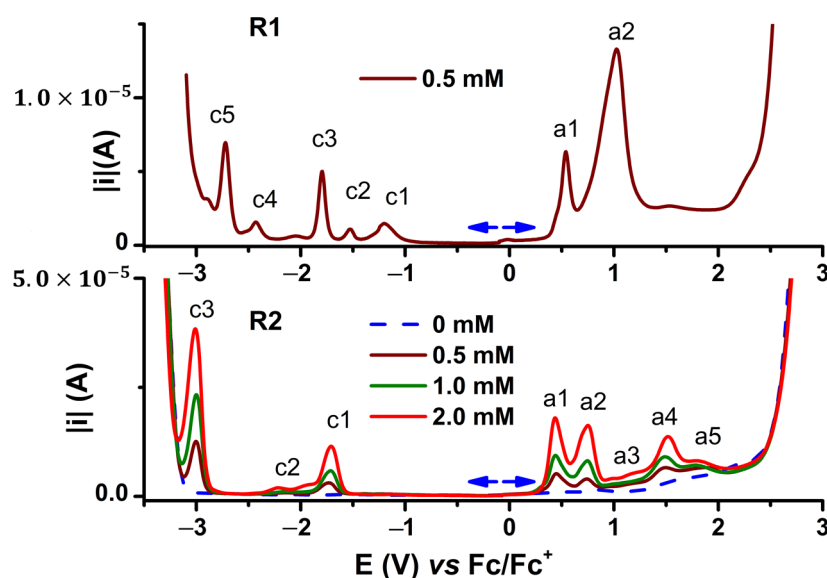


Figure 5. DPV curves (with anodic and cathodic currents in absolute values) for **R1** and **R2** solutions in 0.1 M TBAP/CH₃CN at different concentrations; a1–a5 and c1–c5 are the anodic and cathodic peaks, respectively.

3.1.3. Characterization of Ligands by Rotating Disk Electrode Voltammetry

In Figure 6, the voltammograms obtained by RDE at [**R1**] = 0.25 mM and for [**R2**] = 2 mM, at different rotation rates, are presented in parallel. The voltammograms obtained at a rotation rate of 1000 rpm for different concentrations of **R1** and **R2** are presented in Figure 7. To correlate the processes that were highlighted in RDE and DPV, the voltammograms

obtained for **R2** ligand are represented in parallel in Figure S4. Figure S5 shows in detail for $[R2] = 1 \text{ mM}$ the appearance of an anodic process evident at approximately 2 V, which decreased with increasing electrode rotation rate. Table 2 shows the values for the anodic and cathodic processes for **R2** at a concentration of 2 mM by the previously listed electrochemical methods.

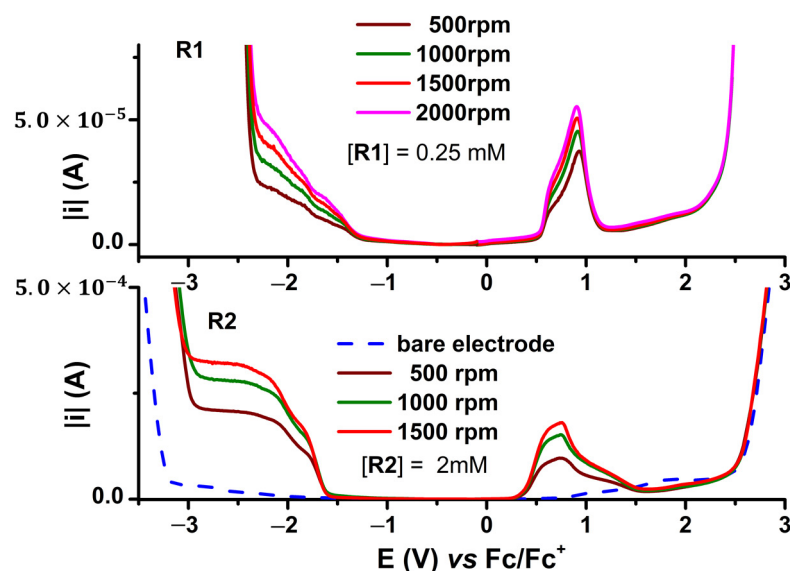


Figure 6. RDE curves on GC for $[R1]$ and $[R2]$ solutions in 0.1 M TBAP/ CH_3CN ; the cathodic currents are plotted in absolute values.

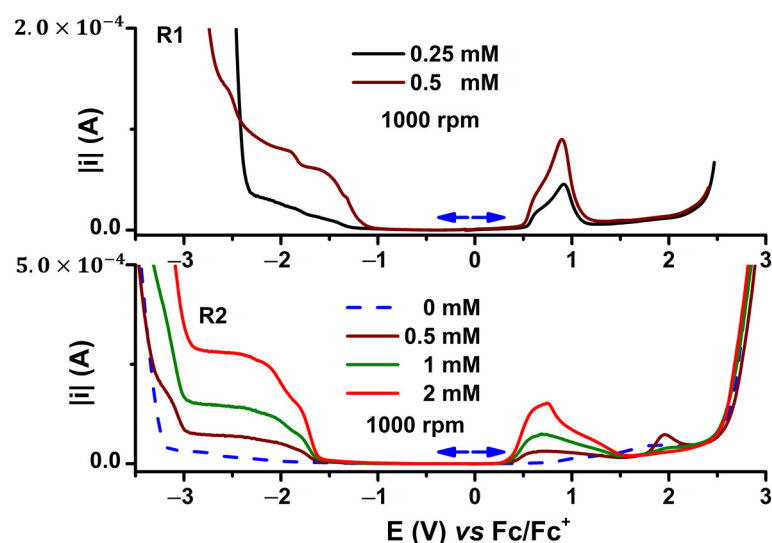


Figure 7. RDE curves on GC at 1000 rpm for $[R1]$ and $[R2]$ solutions at different concentrations in 0.1 M TBAP/ CH_3CN ; the cathodic currents are in absolute values.

3.2. Preparation and Electrochemical Characterization of Modified Electrodes Based on the Aromatic Rhodanine

The electrochemical immobilization of **R2** ligand on the glassy carbon electrode was carried out in millimolar solutions of the ligand by scanning or CPE at potentials close to those of the anodic processes, as shown in previous works [20,26,32–35]. After obtaining the chemically modified electrodes based on **R2** (**R2**-CME), each electrode was rinsed with acetonitrile and transferred to ferrocene (Fc) solution in 0.1 M TBAP/ CH_3CN . The CV curves of Fc obtained on the CMEs in different conditions were compared with those obtained on the unmodified electrode, and the differences were analyzed.

3.2.1. Formation of Modified Electrodes Based on the Aromatic Rhodanine by Scanning

Figure 8 shows the evolution of the CV curves during successive scans in the domain of processes a1–a5. The comparison of the CV curves recorded in transfer solution of Fc on the obtained CMEs and uncoated GC (Figure 6) suggested the formation of thin films. Figure 9 shows the evolution of potentials and peak currents on the obtained modified electrodes.

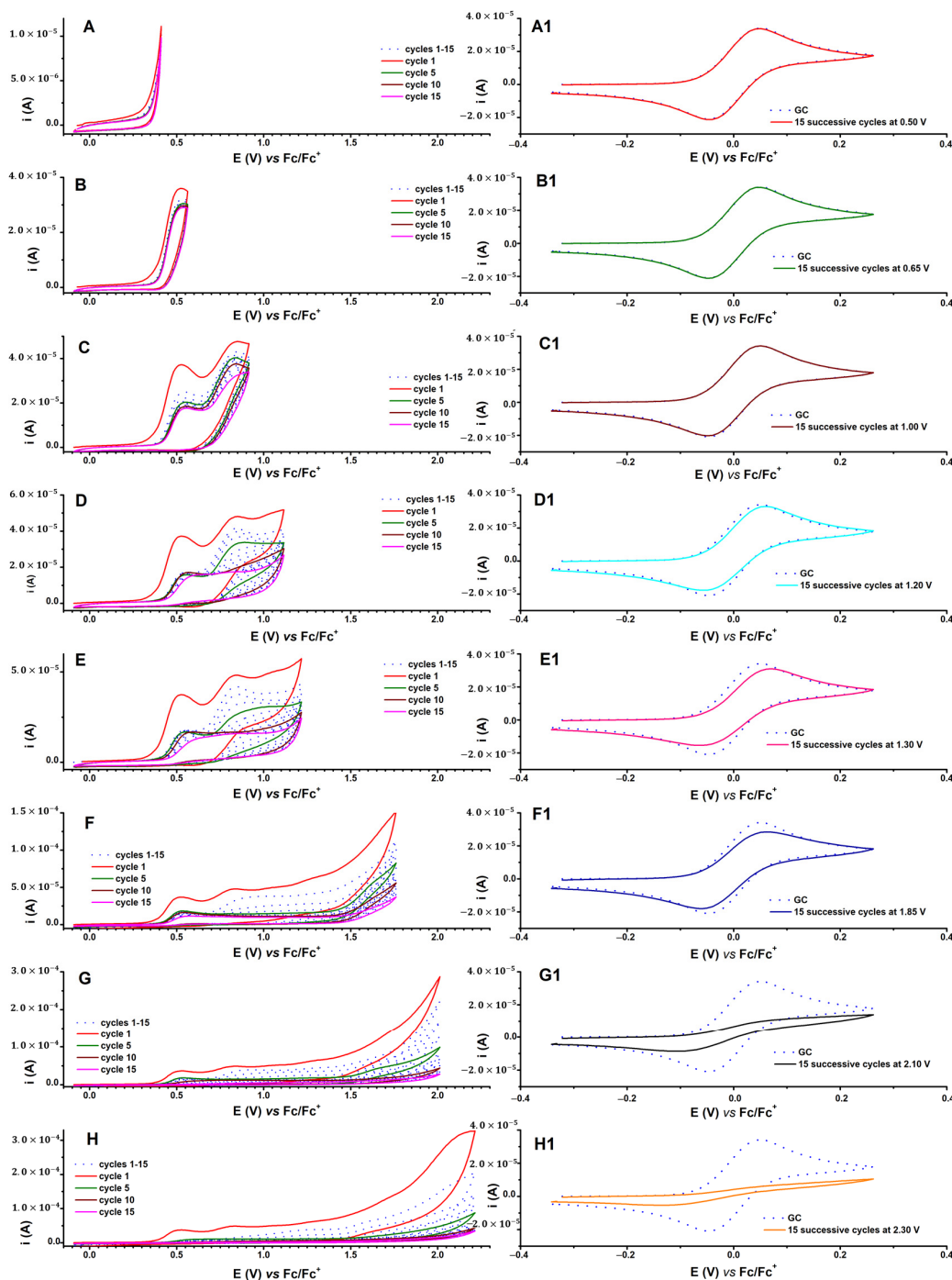


Figure 8. Successive CV cycles (0.1 V/s) in R2 solution (2 mM) in 0.1 M TBAP/CH₃CN carried out during the synthesis of CMEs by scanning at different anodic limit potentials (V) increasing in the order: (A) < (B) < (C) < (D) < (E) < (F) < (G) < (H) (left side), and the curves in 1 mM Fc solution in 0.1 M TBAP/CH₃CN of the corresponding CMEs vs. bare electrode (dashed lines) (right side).

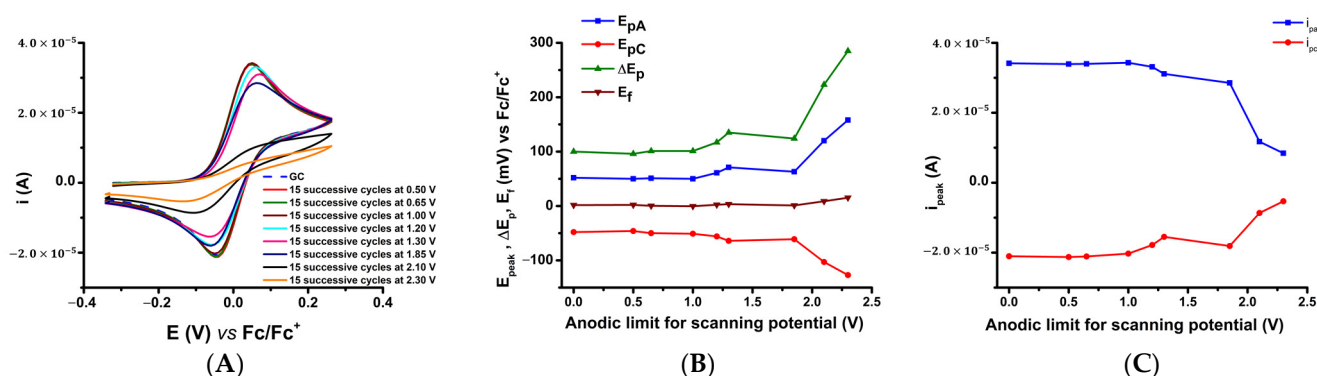


Figure 9. Analysis of **R2**-CME film formation by scanning: cumulated CV curves (0.1 V/s) after the transfer of **R2**-CMEs in 1 mM Fc solution in 0.1 M TBAP/CH₃CN vs. bare electrode (A), variations of E_{pa} (blue), E_{pc} (red), ΔE_p (olive), and E_f (wine) (B), and of i_{pa} (blue) and i_{pc} (red) vs. anodic limit for scanning potential (C).

3.2.2. Formation of Modified Electrodes Based on the Aromatic Rhodanine by Controlled Potential Electrolysis

The chemical immobilization of the ligand by CPE was performed from solutions of **R2** in 0.1 M TBAP/CH₃CN with a concentration of 2 mM. The corresponding chronoamperograms are given in Figure S6. When the modified electrodes were obtained by CPE, their transfer in Fc solution led to the CV curves shown in Figure 10A. Figure 10B,C show the evolution of peak potentials and currents for Fc on the obtained CMEs.

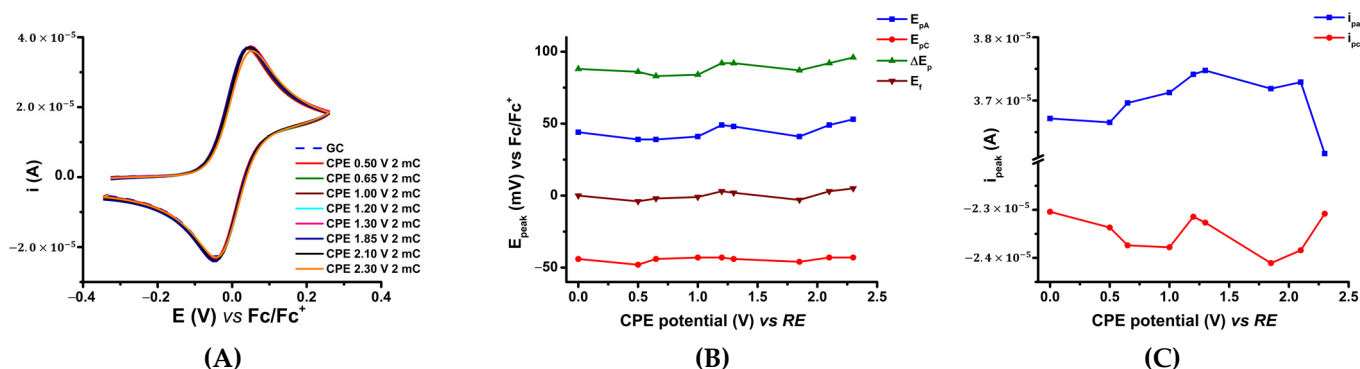


Figure 10. Analysis of **R2**-CME film formation by CPE: cumulated CV curves (0.1 V/s) on **R2**-CMEs after the transfer in 1 mM Fc solution in 0.1 M TBAP/CH₃CN vs. bare electrode (A); plots of E_{pa} (blue), E_{pc} (red), ΔE_p (olive), and E_f (wine) vs. CPE potential (B), and of i_{pa} (blue) and i_{pc} (red) vs. CPE potential (C).

3.3. Heavy Metal Recognition Experiments Using Modified Electrodes Based on the Aromatic Rhodanine

In order to compare the electrodes modified with the two ligands, the recognition of HM ions on electrodes modified with **R2** was realized. **R2**-CMEs were obtained by CPE from millimolar solutions of **R2** in 0.1 M TBAP/CH₃CN. Figure 11 shows the stripping curves obtained by DPV recorded on **R2**-CMEs prepared from **R2** and immersed in mixed solutions with different concentrations (for 10 min accumulation times). Figure 12A shows the dependence of the area of the stripping peak currents for each metallic ion that was present in the accumulation solutions. The DPV peak current dependence on Pb concentration is shown in Figure 12B. Figure 13 shows in parallel the DPV stripping curves recorded on modified electrodes based on **R1** and **R2** to highlight the difference between the two ligands.

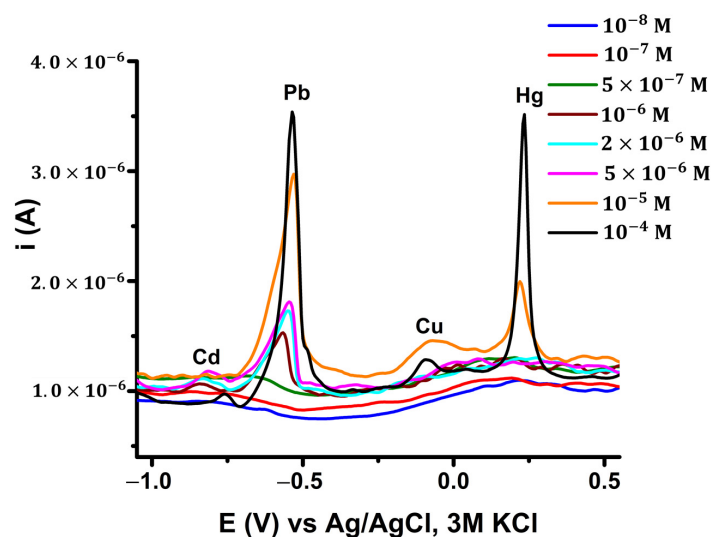


Figure 11. DPV curves recorded on R2-CMEs (obtained by CPE at 1.3 V and 2 mC) for different concentrations of mixed metals in the accumulation solutions at 10 min accumulation times.

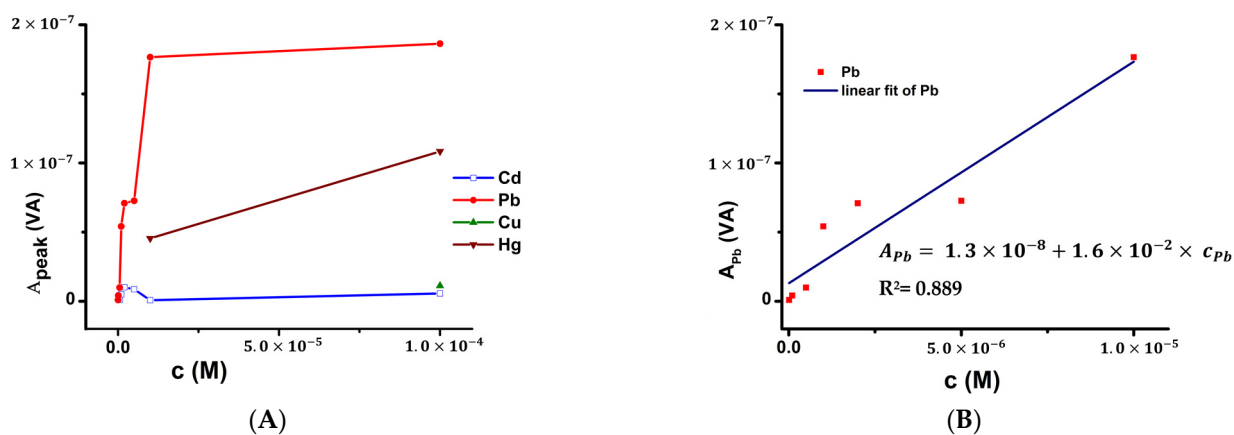


Figure 12. Dependence of DPV stripping peak area on the metallic ion's concentration for each ion (A), and on Pb ion concentration in the linear dependence range (B).

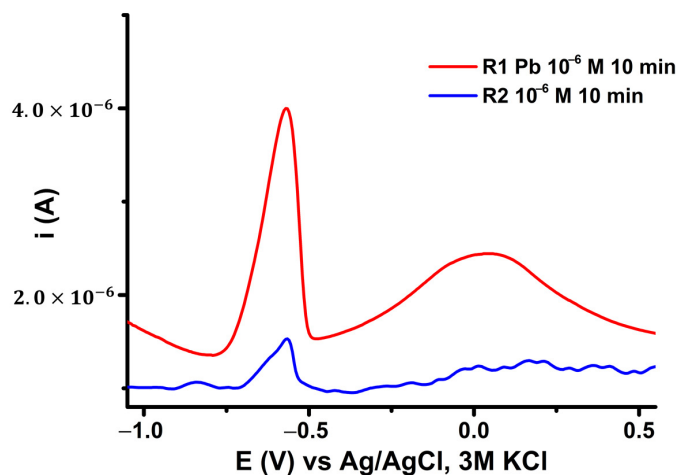


Figure 13. DPV curves (0.01 V s^{-1}) for CMEs obtained by CPE (at 1.3 V, 2 mC for R2 and 1.2 V, 0.7 mC for R1) after 10 min accumulation times in solution concentrations of 10^{-6} M mixed metals for R2 and 10^{-6} M Pb(II) for R1.

3.4. UV-Vis Study of Pb Complexation in Solution

UV-Vis spectra for different concentrations of **R1** or **R2** were recorded to find the extinction coefficients and main wavelength absorption bands for **R1** and **R2**, respectively. The variation of these spectra in the presence of the investigated HM ions was noticed. The dependence of absorbance on monomer concentration was recorded to find the stoichiometric ratio of the formed complexes. Figure S7 shows the UV-Vis spectra obtained for different concentrations of **R1** and its inset gives the dependence of absorbance on **R1** concentration for different wavelengths given in Table 3. Figure 14 shows the UV-Vis spectra for different $[Pb^{2+}]/[R1]$ ratios and the variation of the absorbance for the peak at 457 nm vs. $[Pb^{2+}]/[R1]$ ratio (I1 inset) and vs. $[Pb^{2+}]/([Pb^{2+}] + [R1])$ molar fraction (I2 inset). Figure S8 gives the UV-Vis spectra obtained for different concentrations of **R2** for different wavelengths and the linear dependence of UV-Vis peak absorbance on concentration in the inset, which is given in Table 4. Figure 15 gives the UV-Vis spectra for different $[Pb^{2+}]/[R2]$ ratios and the variation of the absorbance for the peak at 474 nm vs. $[Pb^{2+}]/[R2]$ ratio (I1 inset) and vs. $[Pb^{2+}]/([Pb^{2+}] + [R2])$ molar fraction (I2 inset). The ratios r/m for $(Pb)_m(R1)_r$ and $(Pb)_m(R2)_r$, according to the Mollard method for absorbance (A), are given in Tables S3 and S4, respectively.

Table 3. Linear dependence of absorbance peaks for **R1**.

Maximum Wavelength, nm ¹	Equation	Adj. R-Square
$\lambda_1 = 457$	$A_{\lambda_1} = 0.01446 + 0.02962 \times c$	0.998
$\lambda_2 = 435$	$A_{\lambda_2} = 0.03176 + 0.02947 \times c$	0.988
$\lambda_4 = 289$	$A_{\lambda_4} = 0.02533 + 0.01688 \times c$	0.969
$\lambda_5 = 231$	$A_{\lambda_5} = 0.0188 + 0.01642 \times c$	0.964

¹ for λ_3 , maximum values could not be read for all calibration determinations.

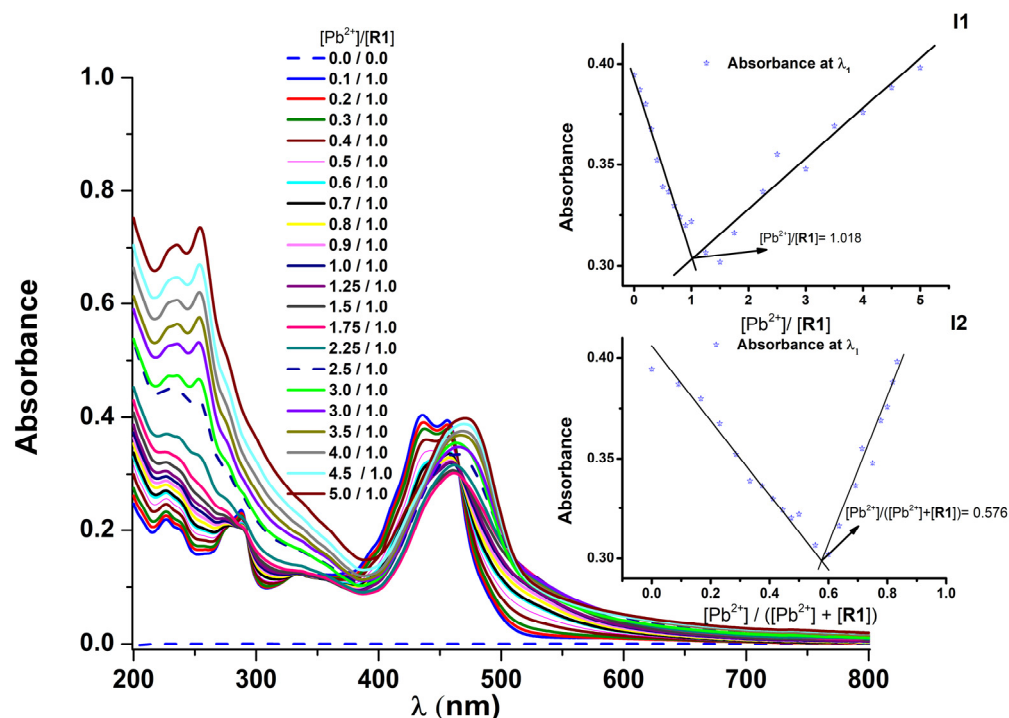
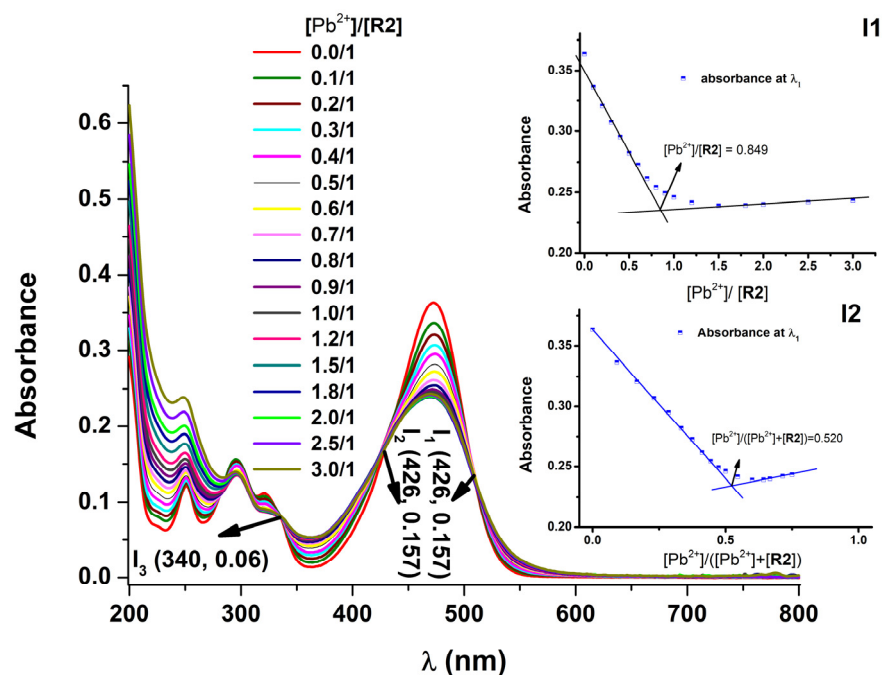


Figure 14. UV-Vis spectra (recorded after 1 min) for various $[Pb^{2+}]/[R1]$ ratios; insets: variation of the absorbance for the peak at 457 nm vs. $[Pb^{2+}]/[R1]$ (I1 inset) and vs. $[Pb^{2+}]/([Pb^{2+}] + [R1])$ (I2 inset).

Table 4. Linear dependence of absorbance peaks for **R2**.

Maximum Wavelength, nm	Equation	Adj. R-Square
$\lambda_1 = 474$	$A_{\lambda_1} = -0.02161 + 0.06887 \times c$	0.992
$\lambda_2 = 321$	$A_{\lambda_2} = 0.00573 + 0.01793 \times c$	0.994
$\lambda_3 = 295$	$A_{\lambda_3} = 0.00953 + 0.02491 \times c$	0.993
$\lambda_4 = 251$	$A_{\lambda_4} = 0.00083 + 0.02139 \times c$	0.993

**Figure 15.** UV-Vis spectra after 1 min for different $[Pb^{2+}]/[R2]$ ratios; insets: variation of the absorbance for the peak at 457 nm vs. $[Pb^{2+}]/[R2]$ (**I1** inset) and vs. $[Pb^{2+}]/([Pb^{2+}] + [R2])$ (**I2** inset).

4. Discussion

4.1. Comparison between Electrochemical Behavior of the Two Ligands

In the anodic domain, where the relevant peaks are a1 and a2 (Figure 2), the electrochemical behavior evaluated by CV for the ligands **R1** and **R2** in millimolar solutions in the supporting electrolyte was similar. For both ligands, linear dependence of the peak current on the ligand concentration was obtained, certifying the assignment of the peaks to some processes undergone by the ligand (for **R1** according to [32] and for **R2** according to Figure S1 and Table S1).

The dependencies of the peak currents a1 and c1 on the scan rate for both ligands were compared. For **R2**, Figure 3a showed the variation of the CV curves for different scan rates in the domain of processes a1 and c1, while Figure 3b showed the linear dependencies of the peak currents a1 and c1 on the radical of the scan rate, which confirmed a diffusive controlled charge transfer. The slope of the dependence of the anodic peak current a1 (Table 1) for both ligands was similar.

Figure 4 illustrated the character of the **R2** peaks, summarized in Table 2, which was evidenced by CV on different scan domains and scan rates. According to Table 2, the first CV oxidation potential peak a1 for **R2** (0.526 V) was at about the same positive potential as the azulene derivative **R1** (0.579 V) [32]. The second oxidation peak for **R2**, a2, had a similar position with respect to the azulene derivative **R1** (0.84 V vs. 1.143 V [32], respectively). This proved that the amino group in **R2** enabled easy oxidation of the overall molecule compared to a pure aromatic compound such as phenylene-2thioxothiazolidin-4-one. For cathodic processes, the CV c1 peak potential was -1.759 V for **R2** and -1.202 V for **R1** [32]. As expected, it was more difficult to reduce **R2**, which has an amino group.

The DVP peaks a1 and a2 (Figure 5) were situated in good accordance with the peaks registered by CV: 0.436 V and 0.753 V vs. 0.541 V and 1.022 V, respectively (Table 2). Linear dependence of the DPV peak current on concentration was found for both ligands: for **R1** (according to [32]) and **R2** (as shown in Figure S2). Figure S3 showed, with a dashed line, a good correlation between the potential peaks revealed by CV and DPV for **R2**.

The comparative RDE study (Figures 6 and 7) showed a *peak* form for the anodic processes followed by a decrease down to the background values of RDE at potentials in the range of the a1 and a2 peaks. This confirmed the formation of insulating films for both monomers. In the cathodic domain of scanning, the two monomers had regular curves but the reduction potentials were different, being more negative for **R2**. Their half-wave potentials ($E_{1/2}$) taken from the RDE curves were in good agreement with the CV and DPV peak potentials (Table 2). Figure S4, containing a detailed image of the processes for different rotation rates and **R2** concentrations, showed the correspondence between the processes evidenced by DPV and RDE. An evident asymmetry between the anodic and cathodic processes could be noticed, especially for the RDE curves. The anodic currents were much smaller than the cathodic ones due to film formation. This asymmetry was less evident in the DPV curves. With the increased rotation rate in RDE, the signal for the a1 peak increased, while the peak at 1.8 V, denoted as a5 in DPV, decreased (Figure S5). This evolution can be explained by the formation of insulating films at potentials higher than 0.8 V.

4.2. Comparison between the Formation of Chemically Modified Electrodes

This work found the common features of the CMEs in the preparation of **R1**-CMEs and **R2**-CMEs and their electrochemical characterization. This showed the formation of an insulating film either by scanning or CPE for both ligands. For **R2**, Figure 8A–H illustrated the decrease in the oxidation currents in successive cycles during preparation by scanning, which was more pronounced when the anodic limit of the scan increased. The transfer of modified electrodes in Fc solution led to modified CV curves, as shown in Figure 8A1–H1. Their shapes depended on the anodic limit of the scan during the preparation, being flatter for anodic limit values higher than 1 V. The analysis of the Fc signal on these curves, shown in Figure 9A, indicated that the anodic/cathodic potential peak (E_{pa}/E_{pc}) of Fc was constant until 1 V and then it increased in absolute value, whereas the formal potential (E_f) was constant. The difference between E_{pa} and E_{pc} (ΔE_p) was constant until 1 V and then it increased (Figure 9B). The Fc anodic/cathodic peak current i_{pa}/i_{pc} was constant until 1 V and then it decreased in absolute value (Figure 9C). All of these facts confirmed the formation of insulating films when the scanning potential in the preparation was above 1 V.

When the CMEs were prepared by CPE starting from **R2** solutions (as shown in Figure S6), the Fc probe on these CMEs (Figure 10A) had a slight variation with CPE potential. The detailed analysis of the Fc signal on these curves indicated that the anodic/cathodic potential peak (E_{pa}/E_{pc}) and the difference between E_{pa} and E_{pc} (ΔE_p) of Fc were almost constant until 1.8 V, and then they slightly increased in absolute value, whereas the formal potential (E_f) was practically constant (Figure 10B). The Fc anodic/cathodic peak current i_{pa}/i_{pc} slightly increased in absolute value until 1.8 V and then it decreased (Figure 10C). All of these findings supported the formation of thin insulating films. The difference noticed between the two modes of preparation in the case of **R2** can be attributed to the slow formation of films by scanning compared to CPE.

For **R1**, the two preparation modes did not generate such differences [32]. This can be correlated with the well-known polymerization capacity of the azulene moiety in comparison with the aromatic moiety.

4.3. Comparison between Heavy Metal Recognition Properties Using Modified Electrodes

The stripping curves recorded on **R1**-CMEs and **R2**-CMEs for different concentrations of mixed metals (Table 5) showed peaks for each of the metal ions in the accumulation solution at close potentials (Figure 11). Their intensities varied depending on the concentra-

tion. The shape of the obtained peak intensity vs. concentration curves (Figure 12A) was of the type of a *saturation curve* with different limiting currents. Among the metals tested, Pb showed the most intense signals and a relatively wide linear range between 10^{-8} and 10^{-5} M (Figure 12B), as in the case of **R1**-CMEs [32].

Table 5. Potential values (V) for DPV peaks of investigated metals using CMEs based on **R1** and **R2** in accumulation solutions containing mixtures of HMs with concentrations of 10^{-4} M for each ion.

Modified Electrode	Cd	Pb	Cu	Hg
R1 -CME	−0.759	−0.533	−0.094	0.235
R2 -CME	−0.757	−0.533	−0.089	0.235

The stripping curves recorded on **R1**-CMEs and **R2**-CMEs (Figure 13) highlighted the difference between the two ligands in building sensitive CMEs for HMs. Both types of CME achieved better analysis of Pb(II) among the cations investigated, but their selectivity for the involved metal ions was different. **R1**-CMEs were found to be significantly better than **R2**-CMEs, as the Pb stripping area was about eight times larger. This meant that the azulene ligand **R1** was a better ligand than **R2** in the CME-based analysis of Pb.

The values provided in Table 5 showed that the stripping potentials for the cations were practically identical, which proved the similarity of the two rhodanines. This observation differed from other previous experimental conclusions because we obtained different values for the stripping potential of cations when we performed studies with electrodes modified with differently substituted azulenes [32]. The potential difference may be due to the formation of films with different structures due to the specific steric hindrance of each substitution.

4.4. Comparison between Heavy Metal Complexation of the Two Ligands in Solution by UV-Vis

The UV-Vis spectral investigations in micromolar solutions of each ligand revealed specific absorption wavelengths. These allowed the estimation of their extinction coefficients and the obtaining of calibration curves. The results for **R1** and **R2** (Figures S7 and S8, respectively) allowed the identification of the maximum wavelengths presented in Tables 3 and 4, respectively, and the calculation of extinction coefficients for **R1** ($2.95 \cdot 10^9 \text{ M}^{-1} \cdot \text{cm}^{-1}$ for the visible range and $1.66 \cdot 10^9 \text{ M}^{-1} \cdot \text{cm}^{-1}$ for the UV range) and for **R2** ($6.89 \cdot 10^9 \text{ M}^{-1} \cdot \text{cm}^{-1}$ for the visible range and $2.3 \cdot 10^9 \text{ M}^{-1} \cdot \text{cm}^{-1}$ for the UV range).

The absorption bands at longer wavelengths for the **R1** and **R2** derivatives can be associated with a localized $\pi \rightarrow \pi^*$ transition throughout the molecular system. The visible absorption band of **R2** showed a red shift compared to **R1** due to a higher degree of conjugation in **R2**. The absorption bands in the range 220–350 nm for **R1** probably belong to the azulene ring, and the absorption bands around 320, 295, and 250 nm in **R2**, respectively, can be attributed to $\pi \rightarrow \pi^*$ transitions linked to the dimethylaminobenzylidene unit.

Since Pb was found to be well identified using the CMEs, UV-Vis analysis of **R1** or **R2** solutions was performed for Pb. The variation of absorbance in the presence of increasing amounts of Pb showed the possibility of using this technique as an analytical tool based on the homogeneous complexation of Pb by the ligands.

The variation of the UV-Vis spectra for different amounts of metals (Figure 14) allowed the estimation of the ratio between Pb and **R1** in the complex in solution and the establishment of its stoichiometry Pb:**R1** = 3:4, a ratio calculated by two methods (inserts I1 and I2 in Figure 14).

Similarly, the variation of the UV-Vis spectra for different amounts of Pb (Figure 15) allowed the estimation of the ratio between Pb and **R2** in the complex and the establishment of a similar stoichiometry Pb:**R2** = 3:4 (the ratio calculated by two methods according to inserts I1 and I2 from Figure 15).

Although the comparison between **R1** and **R2** regarding Pb complexation by UV-Vis showed similar stoichiometric ratios in complexes for both structures, the higher

extinction coefficient for **R2** than **R1** indicated that **R2** was more efficient in solution for Pb complexation.

The UV-Vis study of these rhodanines provided important information on the role of the rhodanine moiety for optical applications, as has been reported for other rhodanine dyes [36].

5. Conclusions

As azulenic compounds require special conditions during synthesis, the analogy between azulenic derivatives of rhodanine and the aromatic *p*-dialkylaminobenzylidene rhodanine created the premise for easier selection of compounds for certain applications.

Comparison of the electrochemical and optical studies of the azulenic derivative of rhodanine and the aromatic *p*-dialkylaminobenzylidene rhodanine revealed the similarity between the two compounds, which was expected considering their similar electron-donating character. From electrochemical determinations using modified electrodes based on these ligands, the azulene compound was proven to be the best one, in terms of film formation and HM recognition, being about eight times more sensitive than **R2**. The electrodes modified with both rhodanines detected all the metal (Cd, Pb, Cu, Hg) ions in the accumulation solutions, but with the highest intensity for Pb. However, in solution, **R2** was proven to be a good choice for the optical measurement of Pb concentrations, having a higher absorption coefficient. The two ligands had different behaviors in homogeneous or heterogeneous systems.

Supplementary Materials: The following supporting information can be downloaded at: <https://www.mdpi.com/article/10.3390/sym15030752/s1>, Basic properties for the ligand **R1** and characterization by elemental analysis, UV-Vis, ¹H NMR, ¹³C-NMR, IR, MS; Table S1: Equations of CV peak current linear dependence on concentration for **R2**; Table S2: Equations of DPV peak currents linear dependences on concentration for **R2**; Table S3: Calculated r/m ratios for (Pb)_m(**R1**)_r from absorbance (A) values according to the Mollard method; Table S4: Calculated r/m ratios for (Pb)_m(**R2**)_r from absorbance (A) values according to the Mollard method; Figure S1: Dependence of the CV peak current (at the scan rate of 0.1 Vs⁻¹) vs. **R2** concentration; Figure S2: Dependence of peak current for DPV vs. **R2** concentration; Figure S3: DPV and CV (0.1 V/s) curves on GC for **R2** at different concentrations (mM) in 0.1 M TBAP/CH₃CN; Figure S4: DPV (0.01 V/s) (A), RDE at 1500 rpm (B), RDE at 1000 rpm (C), and RDE 500 rpm (D) curves (with currents in absolute values) on GC for **R2** in 0.1 M TBAP/CH₃CN at different concentrations; Figure S5: Anodic RDE curves on GC at different rotation rates (rpm) for [**R2**] = 1 mM in 0.1M TBAP/CH₃CN; Figure S6: Chronoamperograms in coordinates *i*-*t* (A) and *log(i)-t^{-1/2}* (B) during the preparation of **R2**-CME by CPE at different potentials using charges of 2 mC; Figure S7: UV-Vis spectra obtained for different concentrations of **R1** and dependence of absorbance on **R1** concentration (inset); Figure S8: UV-Vis spectra obtained for different concentrations of **R2** and dependence of absorbance on **R2** concentration (inset).

Author Contributions: Conceptualization, E.-M.U. and O.-T.M.; methodology, E.-M.U.; software, G.-O.B.; validation, E.-M.U., M.C. and R.I.; formal analysis, O.-T.M., A.G.B. and C.M.; investigation, O.-T.M. and A.G.B.; resources, M.C.; data curation, G.-O.B., A.C.R. and E.-M.U.; writing—original draft preparation, O.-T.M.; writing—review and editing, E.-M.U. and R.I.; visualization, G.-O.B.; supervision, A.C.R., A.G.B. and G.-O.B.; project administration, E.-M.U. All authors have read and agreed to the published version of the manuscript.

Funding: This research received no external funding.

Acknowledgments: This research was partially supported by Romanian National Authority for Scientific Research, UEFISCDI, under grant PN-III-P2-2.1-PED-2019-0730, contract no. 293PED/2020.

Conflicts of Interest: The authors declare no conflict of interest.

References

1. Anger, V.; Ofri, S. Chemismus der Farbreaktion des Hydrochinons mit Phloroglucin. Neue Tüpfelreaktionen auf Polyhydroxybenzolderivate und Chinone. *Microchim. Acta* **1963**, *51*, 911–919. [[CrossRef](#)]
2. Overholser, L.G.; Yoe, J.H. The Colorimetric Detection and Determination of Palladium with Compounds Containing the p-Nitrosophenylamino Group. *J. Am. Chem. Soc.* **1941**, *63*, 3224–3229. [[CrossRef](#)]
3. Stephen, W.; Townshend, A. Some derivatives of rhodanine as analytical reagents. *Anal. Chem. Acta* **1965**, *33*, 257–265. [[CrossRef](#)]
4. Kaminsky, D.; Kryshchshyn, A.; Lesyk, R. 5-Ene-4-thiazolidinones-An efficient tool in medicinal chemistry. *Eur. J. Med. Chem.* **2017**, *140*, 542–594. [[CrossRef](#)] [[PubMed](#)]
5. Yin, L.J.; Daniel, A.K.; Fung, G.T.; Liang, C.T.; Avupati, V.R. Review of anticancer potentials and structure-activity relationships (SAR) of rhodanine derivatives. *Biomed. Pharmacother.* **2022**, *145*, 112406. [[CrossRef](#)]
6. Baell, J.; Walters, M.A. Chemistry: Chemical con artists foil drug discovery. *Nature* **2014**, *513*, 481–483. [[CrossRef](#)]
7. Dahlin, J.; Walters, M. The essential roles of chemistry in high-throughput screening triage. *Future Med. Chem.* **2014**, *6*, 1265–1290. [[CrossRef](#)] [[PubMed](#)]
8. Baell, J.B. Feeling Nature's PAINS: Natural Products, Natural Product Drugs, and Pan Assay Interference Compounds (PAINS). *J. Nat. Prod.* **2016**, *79*, 616–628. [[CrossRef](#)]
9. Honesty, N.R.; Kardaş, G.; Gewirth, A.A. Investigating Rhodanine film formation on roughened Cu surfaces with electrochemical impedance spectroscopy and surface-enhanced Raman scattering spectroscopy. *Corros. Sci.* **2014**, *83*, 59–66. [[CrossRef](#)]
10. Solmaz, R. Investigation of adsorption and corrosion inhibition of mild steel in hydrochloric acid solution by 5-(4-Dimethylaminobenzylidene) rhodanine. *Corros. Sci.* **2014**, *79*, 169–176. [[CrossRef](#)]
11. Solmaz, R.; Kardaş, G.; Yazıcı, B.; Erbil, M. Inhibition effect of rhodanine for corrosion of mild steel in hydrochloric acid solution. *Prot. Met.* **2005**, *41*, 581–585. [[CrossRef](#)]
12. Solmaz, R.; Kardaş, G.; Yazıcı, B.; Erbil, M. The Rhodanine inhibition effect on the corrosion of mild steel in acid along the exposure time. *Prot. Met.* **2007**, *5*, 476–482. [[CrossRef](#)]
13. Solmaz, R.; Sahin, E.A.; Döner, A.; Kardaş, G. The investigation of synergistic inhibition effect of rhodanine and iodide ion on the corrosion of copper in sulphuric acid solution. *Corros. Sci.* **2011**, *53*, 3231–3240. [[CrossRef](#)]
14. Salci, A.; Solmaz, R. Fabrication of rhodanine self-assembled monolayer thin films on copper: Solvent optimization and corrosion inhibition studies. *Prog. Org. Coat.* **2018**, *125*, 516–524. [[CrossRef](#)]
15. Nho, S.; Kim, D.H.; Park, S.; Tran, H.N.; Lim, B.; Cho, S. Carbazole and rhodanine based donor molecule with improved processability for high performance organic photovoltaics. *Dyes Pigm.* **2018**, *151*, 272–278. [[CrossRef](#)]
16. Fan, M.; Duan, L.; Zhou, Y.; Wen, S.; Li, F.; Liu, D.; Sun, M.; Yang, R. Rhodanine side-chained thiophene and indacenodithiophene copolymer for solar cell applications. *Mater. Today Energy* **2017**, *5*, 287–292. [[CrossRef](#)]
17. Li, G.; Yang, T.; Cheng, H.; Zhang, Y.; Wang, J.; Liu, Y. An investigation of annealing methods for benzodithiophene terthiophene rhodanine based all small molecule organic solar cells. *Org. Electron.* **2020**, *87*, 105904. [[CrossRef](#)]
18. Kardaş, G.; Solmaz, R. Electrochemical synthesis and characterization of a new conducting polymer: Polyrhodanine. *Appl. Surf. Sci.* **2007**, *253*, 3402–3407. [[CrossRef](#)]
19. Wang, L.H.; Jhang, K.B. Electrochemical Preparation of an Au Oxide Electrode and Its Application to Electro-Oxidation of Heterocycles Thiazole. *Electrochemistry* **2012**, *80*, 968–973. [[CrossRef](#)]
20. Matica, O.-T.; Brotea, A.G.; Ungureanu, E.-M.; Mandoc, L.R.; Birzan, L. Electrochemical and spectral studies of rhodanine in view of heavy metals determination. *Electrochem. Sci. Adv.* **2022**, 1–11. [[CrossRef](#)]
21. Liu, R.S.H.; Muthyala, R.S.; Wang, X.S.; Asato, A.E.; Wang, P.; Ye, C. Correlation of substituent effects and energy levels of the two lowest excited states of the azulenic chromophore. *Org. Lett.* **2000**, *2*, 269–271. [[CrossRef](#)]
22. Murfin, L.C.; Lewis, S.E. Azulene—A bright core for sensing and imaging. *Molecules* **2021**, *26*, 353. [[CrossRef](#)]
23. Shevyakov, S.V.; Li, H.; Muthyala, R.; Asato, A.E.; Croney, J.C.; Jameson, D.M.; Liu, R.S.H. Orbital control of the color and excited state properties of formylated and fluorinated derivatives of azulene. *J. Phys. Chem. A* **2003**, *107*, 3295–3299. [[CrossRef](#)]
24. Razus, A.C. Azulene moiety as electron reservoir positively charged systems; A short survey. *Symmetry* **2021**, *13*, 526. [[CrossRef](#)]
25. Kawski, A.; Kukliński, B.; Bojarski, P. Excited state dipole moments of N, N-dimethylaniline from thermochromic effect on electronic absorption and fluorescence spectra. *Chem. Phys.* **2006**, *320*, 188–192. [[CrossRef](#)]
26. Arnold, G.-L.; Lazar, I.G.; Buica, G.-O.; Ungureanu, E.-M.; Birzan, L. New Azulene Modified Electrodes for Heavy Metal Ions Recognition. *Bulg. Chem. Commun.* **2017**, *49*, 205–210.
27. Kshirsagar, V.; Gandhem, S.; Gautam, M.D. Electrochemical studies on p-dimethylaminobenzylidene rhodanine and its application as amperometric reagent. *Rasayan J. Chem.* **2010**, *3*, 772–776.
28. Thamaraiselvi, P.; Duraipandy, N.; Kiran, M.S.; Easwaramoorthi, S. Triarylamine Rhodanine Derivatives as Red Emissive Sensor for Discriminative Detection of Ag⁺ and Hg²⁺ ions in Buffer-Free Aqueous Solutions. *ACS Sustain. Chem. Eng.* **2019**, *7*, 9865–9874. [[CrossRef](#)]
29. Yavuz, E.; Tokalioglu, S.; Sahan, S. FAAS determination of Ag(I) in water, anodes slime, rock and cream samples by solid phase extraction method based on sepa beds SP207/5-(p-dimethylaminobenzilidene) rhodanine combination. *J. Braz. Chem. Soc.* **2013**, *24*, 736–742. [[CrossRef](#)]
30. Diacu, E.; Buica, G.-O.; Chilibon, I.; Birzan, L.; Arnold, G.-L.; Ungureanu, E.-M. Chemically Modified Electrodes Based on 5-(Azulen-1-yl)methylene-2-thioxothiazolidin-4-one. *J. Solut. Chem.* **2016**, *45*, 1588–1597. [[CrossRef](#)]

31. Birzan, L.; Cristea, M.; Draghici, C.C.; Tecuceanu, V.; Maganu, M.; Hanganu, A.; Razus, A.C.; Buica, G.O.; Ungureanu, E.M. Vinylazulenes chromophores: Synthesis and characterization. *Dye. Pigment.* **2016**, *131*, 246–255. [[CrossRef](#)]
32. Ungureanu, E.-M.; Popescu (Apostoiu), M.; Tatu (Arnold), G.-L.; Birzan, L.; Isopescu, R.; Stanciu, G.; Buica, G.-O. Electrochemical Comparison on New (Z)-5-(Azulen-1-Ylmethylene)-2- Thioxo-Thiazolidin-4-Ones. *Symmetry* **2021**, *13*, 588. [[CrossRef](#)]
33. Păun, A.-M.; Matica, O.-T.; Anăstăsoaie, V.; Enache, L.-B.; Diacu, E.; Ungureanu, E.-M. Recognition of Heavy Metal Ions by Using E-5-((5-Isopropyl-3,8-Dimethylazulen-1-yl) Dyazeny)-1H-Tetrazole Modified Electrodes. *Symmetry* **2021**, *13*, 644. [[CrossRef](#)]
34. Enache, L.-B.; Anăstăsoaie, V.; Birzan, L.; Ungureanu, E.-M.; Diao, P.; Enachescu, M. Polyazulene-Based Materials for Heavy Metal Ion Detection. 2. (E)-5-(azulen-1-yldiazenyl)-1H-Tetrazole-Modified Electrodes for Heavy Metal Sensing. *Coatings* **2020**, *10*, 869. [[CrossRef](#)]
35. Pop, M.D.; Brincoveanu, O.; Cristea, M.; Buica, G.O.; Enachescu, M.; Ungureanu, E.-M. AFM and SEM characterization of chemically modified electrodes based on 5-[(azulen-1-yl) methylene]-2-thioxothiazolidin-4-one. *Rev. Chim.* **2017**, *68*, 2799–2803. [[CrossRef](#)]
36. Nakka, N.; Kushavah, D.; Ghosh, S.; Pal, S.K. Photophysical, electrochemical and electron donating properties of rhodanine-3-acetic acid-linked structural isomers. *Chem. Phys.* **2023**, *566*, 111793. [[CrossRef](#)]

Disclaimer/Publisher’s Note: The statements, opinions and data contained in all publications are solely those of the individual author(s) and contributor(s) and not of MDPI and/or the editor(s). MDPI and/or the editor(s) disclaim responsibility for any injury to people or property resulting from any ideas, methods, instructions or products referred to in the content.